A General Model for Amyloid Fibril Assembly Based on Morphological Studies Using Atomic Force Microscopy

Ritu Khurana,* Cristian Ionescu-Zanetti,† Maighdlin Pope,† Jie Li,* Liza Nielson,* Marina Ramírez-Alvarado,‡ Lynn Regan,‡ Anthony L. Fink,* and Sue A. Carter†

Departments of *Chemistry and Biochemistry and †Physics, University of California at Santa Cruz, Santa Cruz, California 95064; and ‡Department of Molecular Biophysics and Biochemistry, Yale University, New Haven, Connecticut 06520-8114

ABSTRACT Based on atomic force microscopy analysis of the morphology of fibrillar species formed during fibrillation of α-synuclein, insulin, and the B1 domain of protein G, a previously described model for the assembly of amyloid fibrils of immunoglobulin light-chain variable domains is proposed as a general model for the assembly of protein fibrils. For all of the proteins studied, we observed two or three fibrillar species that vary in diameter. The smallest, protofilaments, have a uniform height, whereas the larger species, protofibrils and fibrils, have morphologies that are indicative of multiple protofilaments intertwining. In all cases, protofilaments intertwine to form protofibrils, and protofibrils intertwine to form fibrils. We propose that the hierarchical assembly model describes a general mechanism of assembly for all amyloid fibrils.

INTRODUCTION

Amyloidosis is characterized by extracellular protein deposits that form fibrils either in the brain or other organs (Cohen and Jones, 1991). Fibrils from different proteins have surprisingly similar structures on the nanometer scale. Typical fibrils exhibit enhanced fluorescence of the dye thioflavin T (TfT) upon binding, range between 6 and 10 nm in diameter, and show intertwined appearance in negatively stained transmission electron microscope (EM) images (Malinchik et al., 1998). Subfibrillar species, observed at early time points in the aggregation, are believed to assemble into the endpoint fibrils (Goldsbury et al., 1999; Harper et al., 1997; Ionescu-Zanetti et al., 1999).

In recent years, a number of proteins that are not related to disease have been shown to form amyloid fibrils in vitro including acylphosphatase (Chiti et al., 2000), cold-shock protein (Wilkins et al., 2000), hen lysozyme (Krebs et al., 2000), B1 domain of protein G (Ramirez-Alvarado et al., 2000), SH3 domain (Zurdo et al., 2001), cytochrome *c* (Pertinhez et al., 2001), and myoglobin (Fandrich et al., 2001). Each system in which amyloidogenesis can be induced in vitro gives valuable information on the underlying principles of fibril formation. For example, amyloid fibrils are postulated to have high β-sheet content, but native myoglobin contains no β-sheets, whereas insulin has only a small β-strand; this suggests that for these proteins, the secondary structure changes from α to β during conversion to amyloid. Other model systems such as the B1 domain of protein G are important because of our detailed understanding of their folding dynamics.

Amyloid fibril formation generally is a result of alteration of the native conformation. This has been demonstrated for many proteins such as β-amyloid (Aβ) peptides (Barrow and Zagorski, 1991), transthyretin (Kelly et al., 1997), β_2-microglobulin (McParland et al., 2000), lysozyme (Booth et al., 1997), SH3 domain (Zurdo et al., 2001), and immunoglobulin light chains (Khurana et al., 2001). Natively unfolded α-synuclein also undergoes a transition to a partially folded intermediate before fibril formation, again suggesting a role of alternate conformation in fibrillation (Uversky et al., 2001). Partially folded conformations are favored by mutations or changes in the pH and ionic strength and are thought to be critical intermediates in the transition to amyloid fibrils.

The atomic force microscope (AFM) has been used to study the morphology of amyloid fibrils in various proteins including Aβ (Harper et al., 1997; Stine et al., 1996; Blackley et al., 2002), α-synuclein (Conway et al., 2000; Rochet et al., 2000), amylin (Goldsbury et al., 1999), SH3 domain and lysozyme (Chamberlain et al., 2000), and β_2-microglobulin (Kad et al., 2001). Detailed kinetic studies of the fibrillogenesis were previously performed for the variable domain of immunoglobulin light chain (Ionescu-Zanetti et al., 1999) using the AFM to identify the species involved in the assembly process, and a hierarchical assembly model (HAM) was proposed to describe the formation of the fibrils from smaller subspecies. In the present study, the AFM was used to study the morphology of fibrillar species at early and later time points in the protein-aggregation process of three proteins: α-synuclein, insulin, and the B1 domain of protein G. Our results, combined with the data from a number of other structural studies of amyloid proteins, suggest that the previously proposed HAM is of general applicability to amyloid fibril assembly.

Submitted December 28, 2001, and accepted for publication January 28, 2003.

Ritu Khurana and Cristian Ionescu-Zanetti contributed equally to this work.

Address reprint requests to Ritu Khurana, Molecular and Structural Biology Division, Central Drug Research Institute, Lucknow 226001, India. E-mail: ritukhurana2001@yahoo.com or Sue A. Carter, Dept. of Physics, University of California at Santa Cruz, Santa Cruz, CA 95064. E-mail: sacarter@cats.ucsc.edu.

0006-3495/03/08/1135/10 $2.00

The hierarchical assembly model

The essence of this model is that protofilaments form through a nucleated polymerization kinetic model in which the nascent protofilaments elongate through the addition of monomeric, partially folded intermediates to the ends of the growing protofilaments. The rodlike protofilaments then interact with one another to form protofibrils consisting of two (and occasionally three) intertwined protofilaments. Finally, two protofibrils intertwine to form mature fibrils. The protofibrils and fibrils will be much more rigid than the protofilaments, leading to straight, rodlike structures. The driving force for the interactions of protofilaments to protofibrils, and protofibrils to fibrils, as well as the clumping of fibrils, which is often observed, arises from the surface of the protofilaments and involves both hydrophobic and electrostatic interactions. The HAM model predicts that at early times in fibrillation, the predominant fibrillar species will be protofilaments, whereas at later times, only protofibrils and fibrils will be observed. The HAM model predicts that protofibrils and fibrils will exhibit periodicity, as well as potential variations in height due to uneven overlap of the constituent fibrillar species. The periodicity will be a function of the stiffness of the protofilaments and protofibrils. For calcitonin, however, ribbon-shaped fibrils are observed, possibly suggesting that some protofilaments may just interact lengthwise and not necessarily intertwine. The length of the protofilaments is likely determined by the net kinetics of association (elongation) and dissociation of the monomers to the ends of the protofilaments. If protofilaments of different lengths intertwine to form a protofibril, monomers can add to the shorter protofilament to ''fill in'' the protofibril. The HAM model also predicts potential branched fibrillar species; for example, the interaction of two protofibrils to form a fibril could be incomplete, possibly due to intertwining of protofibrils of varying lengths. All of these predictions are borne out in our reported observations.

METHODS

Amyloid fibril formation

α-Synuclein

α-Synuclein (140 amino acids (AA)) was expressed and purified by fusing its gene into an intein/chitin-binding domain system (Impact T7 system from New England Biolabs, Beverly, MA) and expressing the fusion protein in *Escherichia coli* (Uversky et al., 2001). The purity of the resultant protein was assessed by polyacrylamide gel electrophoresis and electrospray mass spectrometry.

A 1.0-mg/mL α-synuclein solution at pH 7.5 in 20 mM Tris, 100 mM NaCl buffer was stirred at 37°C in glass vials with micro stir bars. The α-synuclein solutions were also stirred in the presence of 20–50 μM heparin. Fibril formation started after 24 h and was complete by 36 h as monitored by enhanced TfT fluorescence. We carefully chose conditions where amorphous aggregates and small β-sheet aggregates were not observed, to exclude TfT binding to those intermediates. The presence of fibrils was confirmed by electron microscopy (negative staining with uranyl acetate, data not shown (Uversky et al., 2001)).

Insulin

Purified bovine insulin (51 AA) was provided by Novo Nordisk (Copenhagen, Denmark). Bovine insulin (1 mg/mL) was incubated in 100 mM HCl at pH 1.6 with gentle stirring at 37°C. Fibril formation was monitored for 1–4 h by enhancement in TfT fluorescence in a 10-μM TfT solution of 100 mM Tris. In HCl, insulin exists as a dimer as confirmed by x-ray scattering studies (Nielsen et al., 2001). Again amorphous or other aggregates were not observed at low pH for insulin, and fibril formation was the major pathway. At every hour, 10-μL aliquots of sample were diluted 10-fold to a final concentration of 0.1 mg/mL before deposition on mica.

B1 domain of protein G

The B1 domain of protein G was expressed and purified following published procedures (Smith et al. 1994). Briefly, ion-exchange chromatography (Q-Sepharose) in a gradient of NaCl in 20 mM Tris-HCl buffer (pH 8.0) was followed by gel-filtration chromatography (Hi-Load Superdex 75, Amersham Pharmacia, Uppsala, Sweden) in 50 mM sodium acetate (pH 5.2). Protein purity was checked by polyacrylamide gel electrophoresis, and the protein concentration was determined from the amino acid analysis performed at the Howard Hughes Medical Institute Biopolymer Laboratory and W.M. Keck Foundation Biotechnology Resource Laboratory at Yale University. Fibril formation was complete by 36 h as monitored by enhanced TfT fluorescence. For B1 protein, we started with monomeric protein as confirmed by x-ray crystallography and did not observe aggregates other than fibrils.

AFM imaging

The samples were imaged with an AutoProbe CP AFM (Park Scientific, Sunnyvale, CA). In the AFM, a laser beam is reflected from the top of a small metal cantilever into a split photodiode. When the sharp tip of the cantilever (radius $\approx$ 10 nm) comes into contact with the sample, the deflection of the laser beam can be detected by the difference in the signal from the top and bottom halves of the photodiode. A piezoelectric tube raster scans the sample underneath the tip; it also moves the sample up and down to keep the deflection of the cantilever constant. AFM images are obtained by plotting the z movement as a function of x,y position. The tube scanner was a 100-μm ScanMaster (ThermoMicroscopes). Noncontact Ultralevers (ThermoMicroscopes) were used as cantilevers. Samples were prepared for AFM imaging by drying a 5-μl sample from the reaction mixture on freshly cleaved mica with nitrogen gas. The drying process was less than a minute and did not affect the aggregation status of the sample, because the protofilament elongation and intertwining occurred over several hours. The buffer and salt components were washed from the surface of the mica with double-distilled water, and the mica was dried again. This procedure ensured that the fibrils and protein molecules remained attached to the mica surface possibly due to the slight negative charge on the mica.

The images shown in Figs. 1, 4, and 7 were taken in the noncontact AFM (NC-AFM) imaging mode. NC-AFM is an imaging mode in which the cantilever is set vibrating in the z direction at its resonant frequency of $\sim$100 kHz. The proximity of the sample results in a dampening of the amplitude of vibration of the cantilever. The piezoelectric raster scans the sample and moves it in the z direction to keep the amplitude of vibration constant. The advantage of the NC-AFM imaging mode over the conventional AFM mode described above (contact mode) is that in the former, the tip-sample forces are greatly reduced, which reduces the damage to biological samples. Images were taken in air under ambient conditions at a scan frequency of 1–2 Hz.

Due to the shape of the AFM tip, AFM measurements typically result in broadened widths; however, the shape of the tip does not affect the z-axis measurements. Therefore, accurate heights of fibril species can be determined from AFM measurements. The resolution of the height measurement is mainly limited by the z-axis noise, which is normally a few tenths of

a nanometer under standard imaging conditions. The accuracy of the height measurements is limited by tip-sample interactions that are a function of the imaging conditions; these effects are discussed in more detail (see General characteristics).

Height analysis

Height measurements were made from scan sizes of 5 × 5 μm or less by measuring height profiles normal to the fibril axis over a region greater than the periodicity of height variations and averaging the peak height of the profile. Heights for the different fibril species were obtained by averaging measurements from a large number of individual fibrils (>25), with errors being calculated as one standard deviation (1 σ) from the mean. Fibril periodicity was determined by scanning a line along the length of a fibril and averaging the distance measured between two high points. Measurement results are summarized in Table 1.

RESULTS AND DISCUSSION

To elucidate the mechanism of amyloid fibril formation, the kinetics of fibril formation were monitored by NC-AFM. Samples from both early and late time points in the fibril-formation process were imaged to identify all of the subspecies that are involved. For all three proteins (α-synuclein, insulin, and B1 domain), a very thin species was observed at early time points and classified as a protofilament. At intermediate times, protofibrils, which showed periodic variations in height, were abundant. At longer times, mature fibrils were preponderant. Because thioflavin-T binds to both protofibrils and fibrils, our later time points are not necessarily at the endpoint of the fibril-formation process; this explains why protofibrils are still observed.

Protofilament, protofibril, and fibril dimensions are presented in Table 1. The observations are consistent with the hierarchical assembly model, in which mature amyloid fibrils are assembled by the intertwining of precursor protofilaments and protofibrils. For other proteins, a number of groups have also observed that the mature fibrils result from intertwining of smaller fibrillar species: for Alzheimer's β (1–40) and (1–42), respectively), the intertwining of protofilaments (2.5–3.0 nm in diameter) into fibrils has been observed (Harper et al., 1997; Malinchik et al., 1998).

Several groups have suggested that amyloid fibrils are formed from partially folded intermediate states (Barrow and Zargorski, 1991; Kelly et al., 1997; Booth et al., 1997; Khurana et al., 2001; Uversky et al., 2001). The B1 domain of protein G has been shown to have the greatest propensity to form fibrils when there are many intermediate states sampled during the unfolding transition (Ramírez-Alvarado et al., 2000). For α-synuclein (Uversky et al., 2001) and insulin (Nielsen et al., 2001), changes from their unfolded and native conformations, respectively, are essential before the formation of amyloid fibrils. In the present work, stirring of the proteins under different conditions of pH and temperature led to in vitro fibril formation, which was monitored by enhanced fluorescence of TfT. Various conditions lead to nonnative conformations due to partial unfolding of proteins with exposed hydrophobic regions that are normally masked in the native conformation. Our results suggest that the nonnative monomers interact with each other and form protofilaments. We observe elongation of protofilaments at early time points. After the initial elongation, the average lengths of protofilaments do not change much. In fact, the average protofilament length is comparable to the average lengths of protofibrils and fibrils.

The protofilaments intertwine into protofibrils, and these in turn intertwine to form fibrils. Protofilaments may intertwine to form protofibrils in an effort to minimize the exposure of their hydrophobic regions. We note that our data does not necessarily preclude the possibility that new protofilaments templating off the sides of existing protofilaments. The periodicity observed in protofibrils is expected to be driven by a balance between mechanical forces dominated by the elasticity of the protofilament and the electrostatic forces due to the distribution of hydrophobic regions and charges along the protofilament backbone. Protofibrils

TABLE 1 Dimensions of fibrillar species observed by AFM for four different proteins

Protein	Protofilaments (nm)*	Protofibrils/fibrils (nm)†	Amino acid content (monomer dimensions)‡
α–Synuclein	3.8 ± 0.6	6.5 ± 0.6 (100–150 nm) 9.8 ± 1.2	140 aa (natively unfolded, dimensions not available)
Insulin	1.2 ± 0.3	1.9 ± 0.3 3.0 ± 0.4, 4.8 ± 0.4	51 aa (3.1 × 3.3 × 2.2 nm)
B1 domain of protein G	1.9 ± 0.9	3.9 ± 0.3, 5.2 ± 0.3	58 aa (3.5 × 2.2 × 2.0 nm)
Ig variable-domain SMA§	2.5 ± 0.4	4.5 ± 0.5, 5.9 ± 0.6, 8.0 ± 1.0 (60 nm, 110 nm)	114 aa (4.0 × 2.5 × 1.4 nm)

*Protofilament diameters as inferred from protofilament average-height measurements plotted as histograms, and the smallest peak height from the histograms in Figs. 2, 5, and 7 is estimated as protofilament diameter.

†Diameter measurements for higher-order species protofibrils/fibrils, also derived from the histogram peaks. In parenthesis are the periodicities of some species, where available.

‡The amino acid count for each of the proteins and the dimensions of the natively folded conformation, as measured by x-ray crystallography or NMR techniques.

§SMA, initials of the patient whose sequence was used to clone the gene coding for variable domain of Ig light chain.

presumably intertwine to form fibrils to further minimize exposure of hydrophobic regions.

In the following sections, we give a detailed description of fibril formation for each of the three proteins studied.

α-Synuclein

The α-synuclein fibrils varied in length from ~500 nm to 2.5 μm (Fig. 1, *A* and *B*). Fig. 1 *A* shows a typical protofibril of α-synuclein with an average height of 6.5 nm with high (*red arrow*) and low (*blue arrow*) points of 7.2 and 5.8 nm, respectively. In our preparations, protofibrils also show evidence of intertwining with a periodicity of 100–150 nm and an amplitude (difference in height between high and low points) of ~1 nm (Fig. 1 *A*). Protofilaments, (Fig. 1 *A*, *inset*), protofibrils (Fig. 1 *B*, *red arrow*), and fibrils (Fig. 1 *B*, *blue arrow*) were observed in a variety of different kinetic runs and different samples imaged. A histogram of the heights observed is presented in Fig. 2. The heights of the fibrils observed can be classified into three categories: protofilaments, 3.8 ± 0.6 nm; protofibrils, 6.5 ± 0.6 nm; and fibrils, 9.8 ± 1.2 nm (Fig. 2, *arrows*). Protofilaments (3.8-nm species) were only observed under conditions where heparin was present while stirring α-synuclein solutions (Fig. 2, *solid bars*), and portions of protofilaments were most likely covered with heparin molecules. It is possible that charges on synuclein molecules bind heparin molecules and get stabilized as protofilaments, whereas in the absence of heparin, the protofilaments are highly charged and quickly intertwine with other protofilaments to yield stable protofibrils (6.5-nm species) that are readily observed under all conditions. We note that comparable heights for α-synuclein fibrils (between 8 and 9 nm) were observed when imaged in water rather than air (J. Li, M. Zhu, A. Manning-Bog, A. Donato, D. DiMonte, A. L. Fink, unpublished observations.

Rochet et al. (2000) also looked at fibril morphology and observed one fibril species that shows periodicity along the fibril and is 7.6 ± 0.6 nm at the high points. This species appears to be equivalent to our protofibrils, which are ~7.2 nm at the high points and have an average height of 6.5 ± 0.6 nm (see Fig. 1*A*). Rochet and co-workers also observed fibrils of 12.1 ± 0.9 nm in diameter by EM (Rochet et al., 2000), which might correspond to the fibrils we observed by AFM, with an average height of 9.8 ± 1.2 nm.

The hierarchical assembly model postulates that higher-order fibrils result from the intertwining of a number of protofilaments that behave like stiff rods, having a periodicity to diameter ratio of ~10. In this scheme, protofibrils would be a result of the intertwining of two protofilaments. Thus the high points of protofibril will be 2*D* (where *D* is

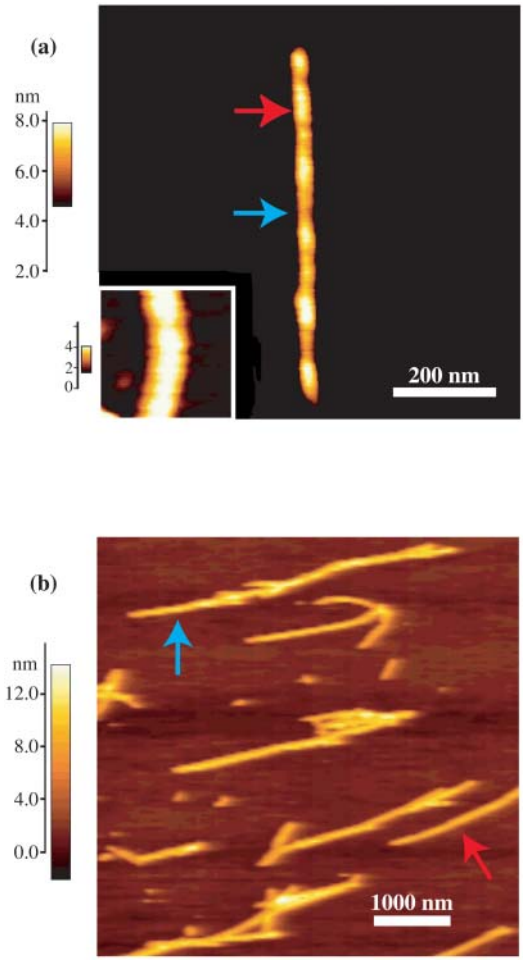

FIGURE 1 AFM images of α-synuclein fibrillar aggregates. (*A*) The observed periodicity of 100–150 nm along the protofibril is shown. The peak (*red arrow*) to trough (*blue arrow*) height difference was ~1 nm, and the average protofibril diameter was 6 nm. (*A*, *inset*) A section of a protofilament with an average height of 3.8 nm. (*B*) A number of juxtaposed fibrillar species: protofibrils of 6.5 nm in height (*red arrow*) and fibrils of 9.8 nm in height (*blue arrow*) are shown adsorbed to the substrate.

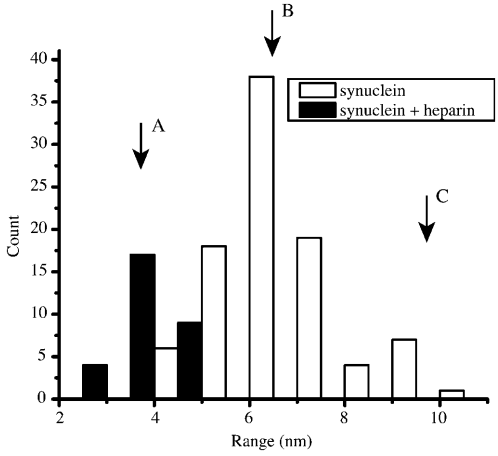

FIGURE 2 A histogram of height distributions of the observed α-synuclein fibrillar species for a number of early and later time points. The three peaks correspond to: (*A*) 3.8-nm protofilaments, (*B*) 6.5-nm protofibrils, and (*C*) 9.8-nm fibrils.

the protofilament diameter), whereas the low points will be ~1.5*D* (due to the stiffness and intertwining, the protofilaments are most likely raised from the surface of mica at the low points), resulting in the measured average height of protofibrils at 1.75*D*. For α-synuclein data, the protofilament diameter *D* is 3.8 nm, yielding an average protofibril diameter of 6.65 nm. This is in excellent agreement with the measured protofibril height of 6.5 ± 0.6 nm. Similarly, intertwining of two protofibrils (6.5 nm in diameter) gives an average fibril height of 11 nm, which is also within σ of the measured value (Fig. 2). This agreement of height measurements, together with the evidence of height variations for the protofibrils and fibrils, suggests a good fit of α-synuclein fibril assembly to the protofilament-intertwining model. A schematic diagram of the resulting paradigm for assembly of α-synuclein into fibrils is presented in Fig. 3.

Insulin

Insulin fibrils were formed in vitro by stirring the protein in an acid solution (pH 1.6). Under these conditions, insulin fibrils reach maturity after 4 h of incubation, after which no further enhancement of TfT fluorescence is observed. In the 1-h incubations, protofilaments (1.2 ± 0.3 nm in diameter, *red arrows*), protofibrils (1.9 ± 0.3 nm, *blue arrows*), and fibrils (3.0 ± 0.4 nm) are observed (Fig. 4 *A*). After 3 h of incubation, both fibrils (*green arrows*) and protofibrils (*blue arrows*) are observed, but no protofilaments (Fig. 4*B*). Large bundles of fibrils (Fig. 4*B*, *white arrow*) were also observed.

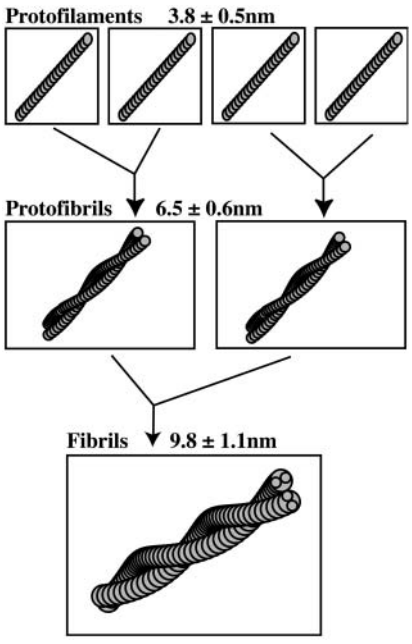

FIGURE 3 A model for the hierarchical assembly of α-synuclein into amyloid fibrils. Protofilament pairs wind together to form protofibrils, and each two protofibrils wind to form a fibril.

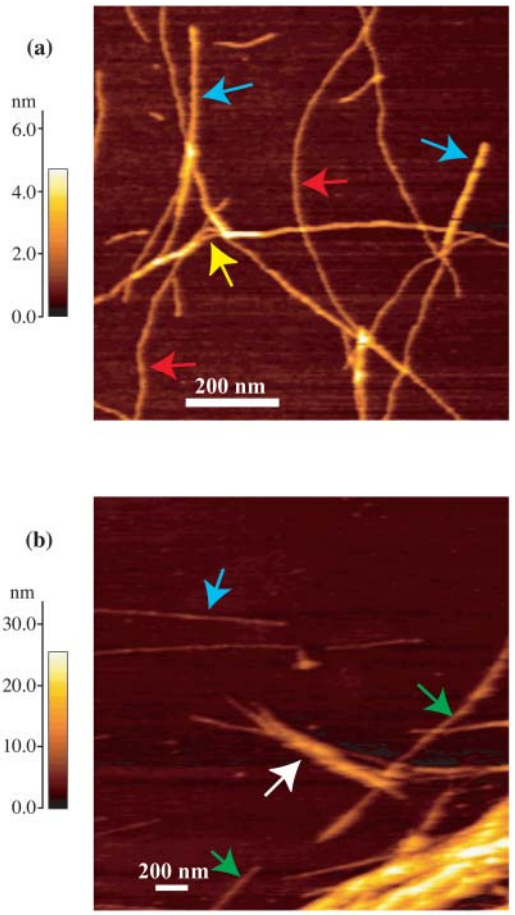

FIGURE 4 AFM images of insulin fibrillar species at two different time points of aggregation. (*A*) Protofilaments (1.2 nm, *red arrows*) and protofibrils (1.9 nm, *blue arrows*) present after 1 h of incubation. Protofilament intertwining to form protofibrils is also observed (*yellow arrow*). (*B*) Protofibrils (1.9 nm, *blue arrows*) and fibrils of various dimensions (*green arrows*) present after 3 h of incubation. A fibril bundle of 50 nm height is also present (*white arrow*).

EM studies of insulin fibrillation report fibril diameter ranging from 3 to 15 nm (Brange et al., 1997). In some cases, protofibrils (3 nm) are seen to bundle together in groups of 2–5 and yield mature fibrils that are 10–15 nm in diameter (Brange et al., 1997).

Our AFM measurements of different fibrillar species of insulin are summarized in the histogram of Fig. 5. The histogram of average fibril heights contains data from both the 1- and 3-h incubations, which are identified as solid and open bars, respectively, in Fig. 5. Peaks in the distribution are taken to be the height of each of the fibrillar species (Fig. 5, *arrows*). The lowest peak is at 1.2 ± 0.3 nm and corresponds to protofilaments. Because the height of the protofilaments is lower than the dimensions of globular natively folded insulin, we conclude that the monomers incorporated into protofilaments have undergone structural changes from the native conformation. It should be noted, however, that dimensions may be underestimated by NC-

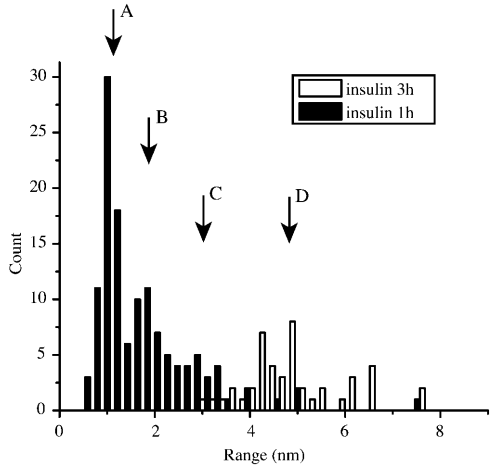

FIGURE 5 The height distributions of insulin fibrillar species are divided into two parts. Measurements of images taken at an early time point (1 h) contain mostly protofilaments (1.2 nm) and protofibrils (1.9 nm). At a later time point (3 h), only fibrils of various dimensions are observed. Peaks in the distribution correspond to: (*A*) protofilaments, (*B*) protofibrils, (*C*) type I fibrils, and (*D*) type II fibrils.

AFM imaging in air due to deformation of the biomolecule by the AFM tip; this effect is discussed further in General characteristics.

Protofibrils, the next stage in fibril assembly, are observed to result from the intertwining of two protofilaments as shown in Fig. 4*A* (*yellow arrow*). Many of the fibrils observed correspond to a protofilament height in one region and a protofibril at one end, which is presumably a result of the intertwining of two protofilaments of unequal length.

Although protofibrils and fibrils are essentially straight over long distances (>500 nm), protofilaments are less rigid and often have a radius of curvature of ~400 nm (Fig. 4*A*, *red arrows*). Clearly, much of the rigidity of the mature fibrils is a result of the increased stiffness due to winding of protofibrils and protofilaments. If two protofilaments intertwine together to form a protofibril, the model predicts average protofibril heights of 1.75*D* (where *D* is the insulin protofilament height of 1.2 nm) or 2.1 nm. This can be identified as the species observed by AFM of 1.9 ± 0.3 nm in height. Two sizes of mature fibrils were observed: a smaller fibril of 3.0 ± 0.4 nm in diameter, corresponding to the intertwining of two protofibrils (and predicted to have a diameter of 3.3 nm) and a larger-diameter fibril of 4.8 ± 0.4 nm in diameter. We identify these as types I and II fibrils, respectively. The type II fibrils can be explained by the intertwining of two type I fibrils, which would be predicted to give a fibril with a diameter of 5.2 nm. This proposed hierarchical assembly is shown in Fig. 6.

B1 domain of protein G

The B1 domain of the Ig-binding domain of protein G (β_1, 58 AA) is a very well-characterized model system for

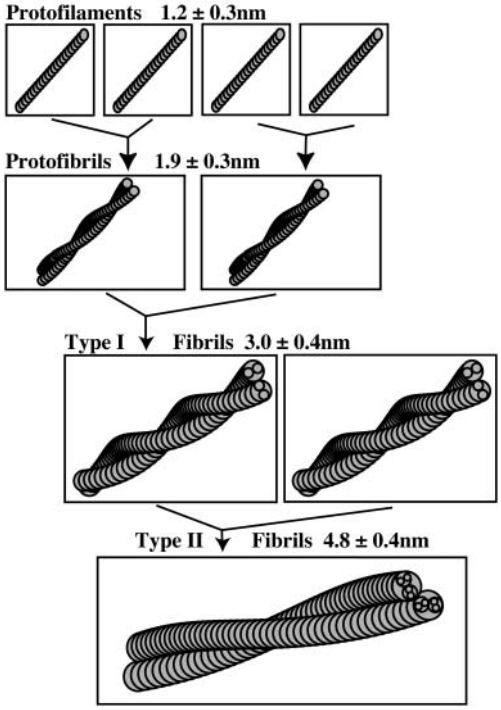

FIGURE 6 A model for the hierarchical assembly of insulin into amyloid fibrils. Protofilament pairs wind together to form protofibrils, and each two protofibrils wind to form a type I fibril. Type II fibrils are the result of winding of type I fibrils.

structural, kinetic, and thermodynamic properties. As shown in previous work (Ramírez-Alvarado et al., 2000), some variants of B1 form fibrils with high reproducibility. It was found that the key requirement for fibril formation is to choose conditions in which the population of intermediate conformations present during the unfolding transition is maximized (Ramírez-Alvarado et al., 2000). As our model system, we chose B1 variants (G6Y53, I6T53) that lead to reproducible fibril formation. Both variants formed fibrils that were indistinguishable from one another by the AFM.

As for α-synuclein and insulin, we observed small protofilaments for B1 variants at early times in the aggregation (24 h; Fig. 7 *A*) that were 1.9 ± 0.9 nm in diameter. At the completion of fibrillation (as determined by no further increase in fluorescence of TfT, 36 h), there were two fibrillar species: we consider the species with a diameter of 3.9 ± 0.3 nm to be protofibrils and the species with a diameter of 5.2 ± 0.3 nm to be fibrils. Both protofibrils and fibrils can be observed in Fig. 7 *B*, an AFM micrograph at 36 h. Each species can be seen as a peak in the height-distribution histogram of Fig. 8 (*arrows*).

Following our postulate that the final fibrils are a result of protofilament winding, simple geometrical considerations lead us to conclude that protofibrils are formed by three protofilaments wound together. Fibrils involve six protofilaments, or two protofilaments wound together with a hexagonal cross section leading to a hollow core, as observed for

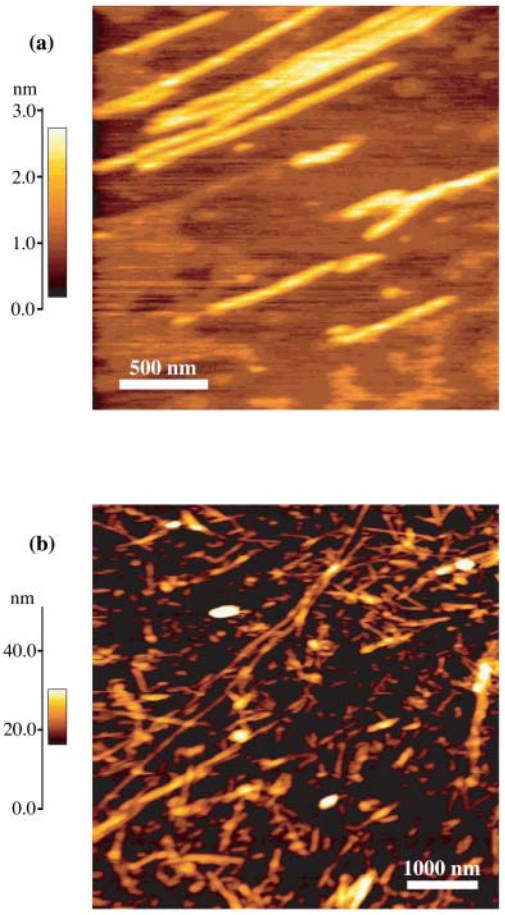

FIGURE 7 AFM images of fibrillar species formed by the B1 domain of protein G. (*A*) Protofilaments (1.9 nm) are observed after incubation for 24 h. (*B*) Protofibrils and fibrils of various diameters and lengths are observed after incubation for 36 h.

SH3 domain fibrils by cryoelectron microscopy; these are also composed of two trimeric protofibrils (Jimenez et al., 1999). In particular, three cylindrical protofilaments wound together have a maximum height of 2*D* (where *D* is the protofilament diameter) and a minimum height of 1.87*D*, leading to an average height of 1.93*D* or 3.7 nm for protofibrils. For six protofilaments arranged in a hexagon, the maximum and minimum heights are 3*D* and 2.72*D*, respectively, and yield an average diameter of 2.85*D* or 5.4 nm. The values are within 1 σ of the measured diameters for protofibrils and fibrils. Alternatively, the fibril could be formed by the winding together of two protofibrils; however, this would require a rearrangement to the hexagonal structure to obtain the same heights. A diagram of the resulting paradigm for assembly of B1 domain protein into fibrils is presented in Fig. 9. A consequence of the model is that it would be difficult to observe the periodicity in the protofibrils and the fibrils, since the difference between the high and low points along the fibril length is small; this may explain why we do not observe any clear periodicity for B1.

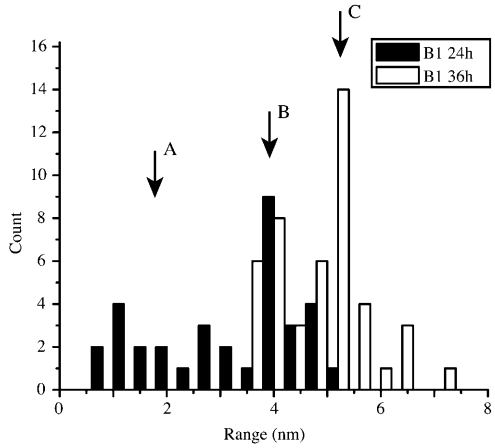

FIGURE 8 Heights of the three different fibrillar species that are present in the B1 aggregates can be extracted from this histogram of observed fibril diameters. Measurements taken at an intermediate time point (24 h) show: (*A*) 1.9-nm protofilaments, (*B*) 3.9-nm protofibrils, and (*C*) 5.2-nm fibrils. Measurements taken at later time points (36 h) show predominantly protofibrils and fibrils of various diameters.

General characteristics

For all three proteins studied, as well as amyloidogenic Ig light chains, we can identify a species that is dominant at early time points in the aggregation and has a small diameter, termed protofilament. Protofilament packing in the mature fibrils differs from one protein to another. Protofilament heights were measured to be from 1.2 (insulin) to 3.5 nm (α-synuclein). We observe a rough correlation between

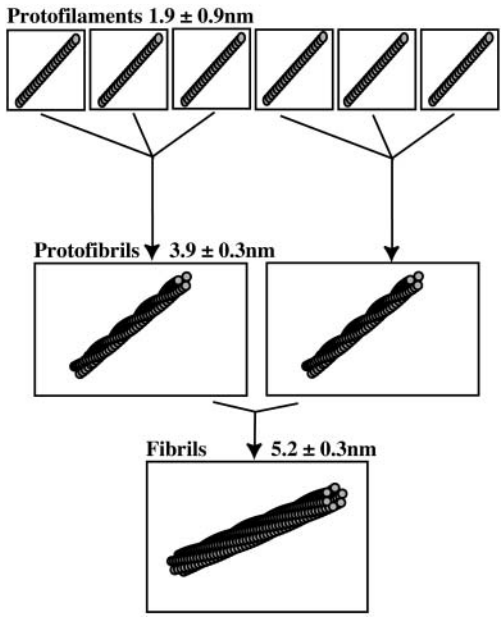

FIGURE 9 A model for the hierarchical assembly of the B1 domain of protein G into amyloid fibrils. Three protofilaments wind together to form a protofibril, and two protofibrils (or six protofilaments) wind to form a fibril.

protofilament size and protein chain length for the proteins included in our study (Table 1). This correlation, however, does not fit other proteins such as amylin (Goldsbury et al., 1999) and Aβ (Harper et al., 1997) possibly due to varying imaging conditions yielding different heights (see discussion below).

Chamberlain et al. (2000) reported a detailed study on amyloid fibrils from an SH3 domain, lysozyme, and a transthyretin peptide using AFM. This study only included the end-time fibrils but still supports our model, since fibrillar species with a broad distribution of heights as well as intertwined fibrils were observed. Chamberlain and coworkers (2000) measured the height of fibrils from a peptide (TTR 10–19) using AFM with both air-dried and buffer samples and also via negatively stained EM. The results for the fibril diameters vary from 6.2 ± 1.5 nm and 5.6 ± 0.6 nm for EM and air NC-AFM, respectively, to as low as 4.4 nm when imaged by NC-AFM in buffer.

These results point out a central issue in the comparison of quantitative results from different laboratories in this field, namely, that although the qualitative fibril-assembly process is common to all observations, the exact dimensions of biomolecules vary depending on the imaging conditions. To complicate matters, careful studies of the height of biomolecules on mica by NC-AFM in buffer show that at least for some biological systems, there is a sharp variability of measured heights as a function of both electrolyte concentration and pH (Müller and Engel, 1997). We have chosen to use NC-AFM in air because samples are stable for long time periods after mica deposition (>20 weeks) and measured heights are in excellent agreement with measurements by high-resolution EM (Ionescu-Zanetti et al., 1999). In addition to providing stability, air drying the sample arrests the kinetics of fibril formation at desired time points.

Other important issues for the comparison of results on the dimensions of fibrillar species are the measurement and reporting methods. Because many of the species observed exhibit a height periodicity along the fibril length, we have performed measurements that average the fibril height over a region that represents at least one period of the height oscillation. Also, for the final determination of the dimensions of fibrillar species, peaks are identified in a histogram of the observed heights, and the peak values are reported along with the standard deviation. This is in contrast with the common practice of simply offering approximate dimensions without determination of the errors involved. Greater homogeneity in the measurement protocols and careful consideration of the effects of imaging conditions on observed heights are clearly important for meaningful comparisons of the results from a number of different studies.

Regardless of the accuracy of the heights, it is easy to confirm the presence of subfibrillar species that assemble into the mature fibrils. For the three proteins studied, we observe that the fibrils are formed by the lateral association of protofilaments. Both protofibrils and fibrils exhibit occasional periodic structures along the fibril length, suggesting protofilaments and protofibrils intertwine to give rise to protofibrils and fibrils, respectively (Fig. 1 *A*). The occasional observation of branch points (Figs. 1 *B* and 4 *A*) and elongation of protofilaments from the ends of protofibrils and fibrils (Fig. 4 *A*) provide additional evidence for protofilament winding as the primary mechanism of fibril assembly. This paradigm is also supported by the fact that single protofilaments are not observed at the endpoints of aggregation (Figs. 2, 5, and 8). This correlates well with observations of twisted structures, branch points, and protofilaments splaying out at the ends of fibrils for a number of systems including Aβ (Harper et al., 1999; Stine et al., 1996; Serpell et al., 2000), SH3 domain and lysozyme (Chamberlain et al., 2000; Zurdo et al., 2001), amylin (Goldsbury et al., 1999), and yeast Sup35 (Xu et al., 2001). Mature fibrils are routinely observed to be composed of 2–6 protofilaments. We should note here that despite the large number of observations that point to the protofilament as the building block of mature fibrils, this is not a universally accepted model. For example, Xu et al. (2001) argue that mature fibrils are formed by the end-to-end addition of large nucleation units, containing perhaps as many as 8–10 monomers; however, it is hard to explain the branching and twisting events that are observed using this model.

The great height variability observed within the protofibril and fibril population is attributed primarily to the different number of constituent protofilaments. In contrast, Chamberlain et al. (2000) ascribe the variability of fibrillar heights to the tightness of the protofibrillar twist. This is based on the interesting observation that larger-diameter fibrils seem to have a shorter periodicity along the fibril length. Although it is clear that this mode of protofibril assembly also plays a role in the final fibril morphology, it is hard to envisage that a doubling of protofibril height is due to a 50% increase in the twist period, since a decrease in the twist period should only bring the height peaks along the fibril closer together rather than increasing both the peak and the trough heights along the fibril.

From the large number of fibrillar precursors observed, these results suggest that the protofilament is the simplest structure and is found at the initial stages of fibrillogenesis. Therefore, we postulate that the protofilaments are the first ordered, insoluble species with a β-sheet core assembled from the monomeric protein. It is possible that the very small dimensions we observe for insulin protofilaments (1.2 nm) might be actually due to their flat placement on the mica, and height measurements may not be the best measure for the diameter of these species. X-ray fiber-diffraction studies (Inouye et al., 1993; Serpell et al., 1995; Serpell et al., 2000) suggest that the core of the fibril is composed of β-strands that run perpendicular to the axis of the fibril, and that the β-strands have a 15° twist to each

other in the ''infinite'' β-sheet that is formed in the direction of the fibril axis. Our data indicate that the diameters of the protofilaments differ for different polypeptides. The apparent variability in protofilament dimensions must be due to a combination of the length of β-strands along with the polypeptide regions that connect the β-strands such as loops and turns. There is evidence for the presence of non-β-regions in amyloid fibrils obtained for various proteins from Fourier transform infrared spectroscopy analysis (R. Khurana, K. A. Oberg, S. Sheshadri, J. Li, and A. L. Fink, unpublished observations). The non-β-sheet regions are presumably responsible for the interactions that drive the assembly of protofilaments into higher-order structures. Because the non-β-sheet regions differ from one protein system to another, this would account for the large variability observed in the dimensions and the hierarchical assembly process for various protofilaments.

This work was supported by grants from the Packard Foundations (to S.A. Carter) and the National Institutes of Health (to A.L. Fink). M. Ramírez-Alvarado is a Human Frontier Science Program postdoctoral fellow.

REFERENCES

Barrow, C. J., and M. G. Zagorski. 1991. Solution structures of beta peptide and its constituent fragments: relation to amyloid deposition. *Science*. 253:179–182.

Blackley, H. K., G. H. Sanders, M. C. Davies, C. J. Roberts, S. J. Tendler, and M. J. Wilkinson. 2000. In-situ atomic force microscopy study of beta-amyloid fibrillization. *J. Mol. Biol.* 298:833–840.

Booth, D. R., M. Sunde, V. Bellotti, C. V. Robinson, W. L. Hutchinson, P. E. Fraser, P. N. Hawkins, C. M. Dobson, S. E. Radford, C. C. Blake, and M. B. Pepys. 1997. Instability, unfolding and aggregation of human lysozyme variants underlying amyloid fibrillogenesis. *Nature*. 385:787–793.

Brange, J., L. Andersen, E. D. Laursen, G. Meyn, and E. Rasmussen. 1997. Toward understanding insulin fibrillation. *J. Pharm. Sci.* 86:517–525.

Chamberlain, A. K., C. E. MacPhee, J. Zurdo, L. A. Morozova-Roche, H. A. Hill, C. M. Dobson, and J. J. Davis. 2000. Ultrastructural organization of amyloid fibrils by atomic force microscopy. *Biophys. J.* 79:3282–3293.

Chiti, F., N. Taddei, M. Bucciantini, P. White, G. Ramponi, and C. M. Dobson. 2000. Mutational analysis of the propensity for amyloid formation by a globular protein. *EMBO J.* 19:1441–1449.

Cohen, A. S., and L. A. Jones. 1991. Amyloid and amyloidosis. *Curr. Opin. Rheumatol.* 4:94–105.

Conway, K. A., J. D. Harper, and P. T. Lansbury. 2000. Fibrils formed in vitro from alpha-synuclein and two mutant forms linked to Parkinson's disease are typical amyloid. *Biochemistry*. 39:2552–2563.

Fandrich, M., M. A. Fletcher, and C. M. Dobson. 2001. Amyloid fibrils from muscle myoglobin. *Nature*. 410:165–166.

Goldsbury, C., J. Kistler, U. Aebi, T. Arvinte, and G. J. Cooper. 1999. Watching amyloid fibrils grow by time-lapse atomic force microscopy. *J. Mol. Biol.* 285:33–39.

Harper, J. D., C. M. Lieber, and P. T. Lansbury. 1997. Atomic force microscopic imaging of seeded fibril formation and fibril branching by the Alzheimer's disease amyloid-beta protein. *Chem. Biol.* 4:951–959.

Harper, J. D., S. S. Wong, C. M. Lieber, and P. T. Lansbury. 1999. Assembly of A beta amyloid protofibrils: an in vitro model for a possible early event in Alzheimer's disease. *Biochemistry*. 38:8972–8980.

Inouye, H., P. E. Fraser, and D. A. Kirschner. 1993. Structure of beta-crystallite assemblies formed by Alzheimer beta-amyloid protein analogues: analysis by x-ray diffraction. *Biophys. J.* 64:502–519.

Ionescu-Zanetti, C., R. Khurana, J. R. Gillespie, T. S. Petrick, L. C. Trabachino, L. J. Minert, S. A. Carter, and A. L. Fink. 1999. Monitoring the assembly of Ig light-chain amyloid fibrils by atomic force microscopy. *Proc. Natl. Acad. Sci. USA*. 96:13175–13179.

Jimenez, J. L., J. I. Guijarro, E. Orlova, J. Zurdo, C. M. Dobson, M. Sunde, and H. R. Saibil. 1999. Cryo-electron microscopy structure of an SH3 amyloid fibril and model of the molecular packing. *EMBO J.* 18:815–821.

Kad, N. M., N. H. Thomson, D. P. Smith, D. A. Smith, and S. E. Radford. 2001. Beta-2 microglobulin and its deamidated variant, N17D form amyloid fibrils with a range of morphologies in vitro. *J. Mol. Biol.* 313:559–571.

Kelly, J. W., W. Colon, Z. Lai, H. A. Lashuel, J. McCulloch, S. L. McCutchen, G. J. Miroy, and S. A. Peterson. 1997. Transthyretin quaternary and tertiary structural changes facilitate misassembly into amyloid. *Adv. Protein Chem.* 50:161–181.

Khurana, R., J. R. Gillespie, A. Talapatra, L. J. Minert, C. Ionescu-Zanetti, I. Millett, and A. L. Fink. 2001. Partially folded intermediates as critical precursors of light chain amyloid fibrils and amorphous aggregates. *Biochemistry*. 40:3525–3535.

Krebs, M. R., D. K. Wilkins, E. W. Chung, M. C. Pitkeathly, A. K. Chamberlain, J. Zurdo, C. V. Robinson, and C. M. Dobson. 2000. Formation and seeding of amyloid fibrils from wild-type hen lysozyme and a peptide fragment from the beta-domain. *J. Mol. Biol.* 300:541–549.

Malinchik, S. B., H. Inouye, K. E. Szumowski, and D. A. Kirschner. 1998. Structural analysis of Alzheimer's beta(1–40) amyloid: protofilament assembly of tubular fibrils. *Biophys. J.* 74:537–545.

McParland, V. J., N. M. Kad, A. P. Kalverda, A. Brown, P. Kirwin-Jones, M. G. Hunter, M. Sunde, and S. E. Radford. 2000. Partially unfolded states of $beta_2$-microglobulin and amyloid formation in vitro. *Biochemistry*. 39:8735–8746.

Müller, D. J., and A. Engel. 1997. The height of biomolecules measured with the atomic force microscope depends on electrostatic interactions. *Biophys. J.* 73:1633–1644.

Nielsen, L., R. Khurana, A. Coats, S. Frokjaer, J. Brange, S. Vyas, V. N. Uversky, and A. L. Fink. 2001. Effect of environmental factors on the kinetics of insulin fibril formation: elucidation of molecular mechanism. *Biochemistry*. 40:6036–6046.

Pertinhez, T. A., M. Bouchard, E. J. Tomlinson, R. Wain, S. J. Ferguson, C. M. Dobson, and L. J. Smith. 2001. Amyloid fibril formation by a helical cytochrome. *FEBS Lett.* 495:184–186.

Ramírez-Alvarado, M., J. S. Merkel, and L. Regan. 2000. A systematic exploration of the influence of the protein stability on amyloid fibril formation in vitro. *Proc. Natl. Acad. Sci. USA*. 97:8974–8984.

Rochet, J. C., K. A. Conway, and P. T. Lansbury, Jr. 2000. Inhibition of fibrillization and accumulation of prefibrillar oligomers in mixtures of human and mouse alpha-synuclein. *Biochemistry*. 39:10619–10626.

Serpell, L. C., M. Sunde, M. D. Benson, G. A. Tennent, M. B. Pepys, and P. E. Fraser. 2000. The protofilament substructure of amyloid fibrils. *J. Mol. Biol.* 300:1033–1039.

Serpell, L. C., M. Sunde, P. E. Fraser, P. K. Luther, E. P. Morris, O. Sangren, E. Lundgren, and C. C. F. Blake. 1995. Examination of the structure of the transthyretin amyloid fibril by image reconstruction from electron micrographs. *J. Mol. Biol.* 254:113–118.

Smith, C. K., J. M. Withka, and L. Regan. 1994. A thermodynamic scale for the beta-sheet forming tendencies of the amino acids. *Biochemistry*. 33:5510–5517.

Stine, W. B. Jr., S. W. Snyder, U. S. Ladror, W. S. Wade, M. F. Miller, T. J. Perun, T. F. Holzman, and G. A. Krafft. 1996. The nanometer-scale structure of amyloid-beta visualized by atomic force microscopy. *J. Prot. Chem.* 15:193–203.

Uversky, V. N., J. Li, and A. L. Fink. 2001. Evidence for a partially folded intermediate in alpha-synuclein fibril formation. *J. Biol. Chem.* 276: 10737–10744.

Wilkins, D. K., C. M. Dobson, and M. Gross. 2000. Biophysical studies of the development of amyloid fibrils from a peptide fragment of cold shock protein B. *Eur. J. Biochem.* 267:2609–2616.

Xu, S., B. Bervis, and M. F. Arnsdorf. 2001. The assembly of amyloidogenic yeast sup35 as assessed by scanning (atomic) force microscopy: an analogy to linear colloidal aggregation? *Biophys. J.* 81:446–454.

Zurdo, J., J. I. Guijarro, J. L. Jimenez, H. R. Saibil, and C. M. Dobson. 2001. Dependence on solution conditions of aggregation and amyloid formation by an SH3 domain. *J. Mol. Biol.* 311:325–340.